JGR Solid Earth

RESEARCH ARTICLE
10.1029/2018JB017258

Special Section:
Slow Slip Phenomena and Plate Boundary Processes

Evaluating the Association Between Tectonic Tremors and Earthquakes in Taiwan From 7 Years Catalogs

Wei Peng[1], Kate Huihsuan Chen[1], and Shinji Toda[2,3]

[1]Department of Earth Sciences, National Taiwan Normal University, Taipei, Taiwan, [2]Department of Geophysics, Graduate school of Science, Tohoku University, Tohoku, Japan, [3]Disaster Science Division, Natural Disaster Research, Tohoku University, Sendai, Japan

Key Points:
- We explore the spatiotemporal association between tremors and earthquakes using 7-year tremor and earthquake catalog
- In a confined distance of 5 km, a greater percentage of earthquakes tend to occur in 5 days prior to the tremors
- A commonly high fluid pressure environment may be needed, to facilitate their interaction

Correspondence to:
K. H. Chen,
katepili@gmail.com

Citation:
Peng, W., Chen, K. H., & Toda, S. (2019). Evaluating the association between tectonic tremors and earthquakes in Taiwan from 7 years catalogs. *Journal of Geophysical Research: Solid Earth*, *124*. https://doi.org/10.1029/2018JB017258

Received 24 DEC 2018
Accepted 23 MAR 2019
Accepted article online 31 MAR 2019

Abstract Knowledge of what governs the interaction between slow- and fast-slip earthquakes is essential to understanding the nature of the earthquake cycle. In southern Taiwan, four major earthquakes (2008 M_w 5.2 Taoyuan, 2010 M_w 6.4 Jiashian, 2012 M_w 5.9 Wutai, and 2016 M_w 6.4 Meinong events) that occurred near the active tremor areas provide a unique opportunity to analyze their spatiotemporal association. With the declustered tremor catalog built in this study, we were able to statistically evaluate the possible association between tremor and mainshock-aftershock sequences in space and time. We found that close-by mainshocks influences tremor's timing in a matter of less than 5 days by short-term triggering, while the 2010 M_L 6.4 Jiashian earthquake appears to be most responsible for such triggering. Assuming a low dip angle thrust faulting mechanism, tremors coincided with small static stress increases (8 kPa) in the 2010 M_L 6.4 Jiashian earthquake. The other three major events, however, caused either negative or neglectable stress changes in the tremor zone. The different responses of the tremors can be explained by coseismic slip-induced static stress change. In this complex tectonic region as a boundary between continental subduction and collision, the interaction between slow- and fast-slip phenomena could be facilitated by a commonly high fluid pressure environment.

1. Introduction

Tectonic tremors have been observed in many major fault zones and are thought to be successive small shear failures at the plate interface (Brown et al., 2009; Ide et al., 2007; La Rocca et al., 2009; Shelly et al., 2006, 2007). Their occurrence is often accompanied by slow-slip events (SSEs) and very low frequency events (VLFs) and represents seismic phenomena occurring below the seismogenic zone. Such events are classified within the same family as slow earthquakes. Mounting evidences suggest that tremor activity is closely related to the processes responsible for generating earthquakes (Chuang et al., 2014; Nadeau & Guilhem, 2009; Shelly, 2009). The family of slow earthquakes such as these, representing slip phenomena along plate boundary faults with low slip rates, is therefore important for the long-term assessment of large earthquake potential. Unlike subduction zones (e.g., Brown et al., 2009; Brudzinski et al., 2010; Obara, 2002; Payero et al., 2008; Peterson & Christensen, 2009; Rogers & Dragert, 2003), transform faults (e.g., Nadeau & Dolenc, 2005; Shelly, 2010; Wech et al., 2012) and some inland areas (e.g., Hutchison & Ghosh, 2017; Ohmi & Obara, 2002) where ambient tremors occur on a known fault plane, the tremors in Taiwan are located in a place where no active faults have been identified. Underneath the southern Central Range of Taiwan, deep-seated tectonic tremors and earthquake clusters are situated close to each other in space and highly correlated in time (Chuang et al., 2014), which provides a rare opportunity to improve our understanding of the physical mechanisms governing different types of slip.

In the study area (box of Figure 1), the M_L 6.3 Baihe earthquake destroyed 10,924 houses with 106 fatalities in 1964 (black star in Figure 1). It was not until 2008 that this area began to produce major earthquakes again. The increase in seismicity rate poses a seismic threat to southern Taiwan and raise awareness in regional seismic hazard. The locations of the recent four major events with focal mechanism are shown in Figure 1. In 2008, an active earthquake sequence occurred close to the tremor zone with mainshock magnitude of M_w 5.2, called Taoyuan earthquake (pink star in Figure 1). The aftershocks reveal a linear structure of NE–SW strike and 45°SE dip, consistent with the focal mechanism of strike = 37°, dip = 48°, and rake = 96. The faulting on the northern extension of the Chishan Fault may be responsible for this Taoyuan earthquake sequence (Shih et al., 2014). In 2010, the M_w 6.4 Jiashian earthquake occurred to the

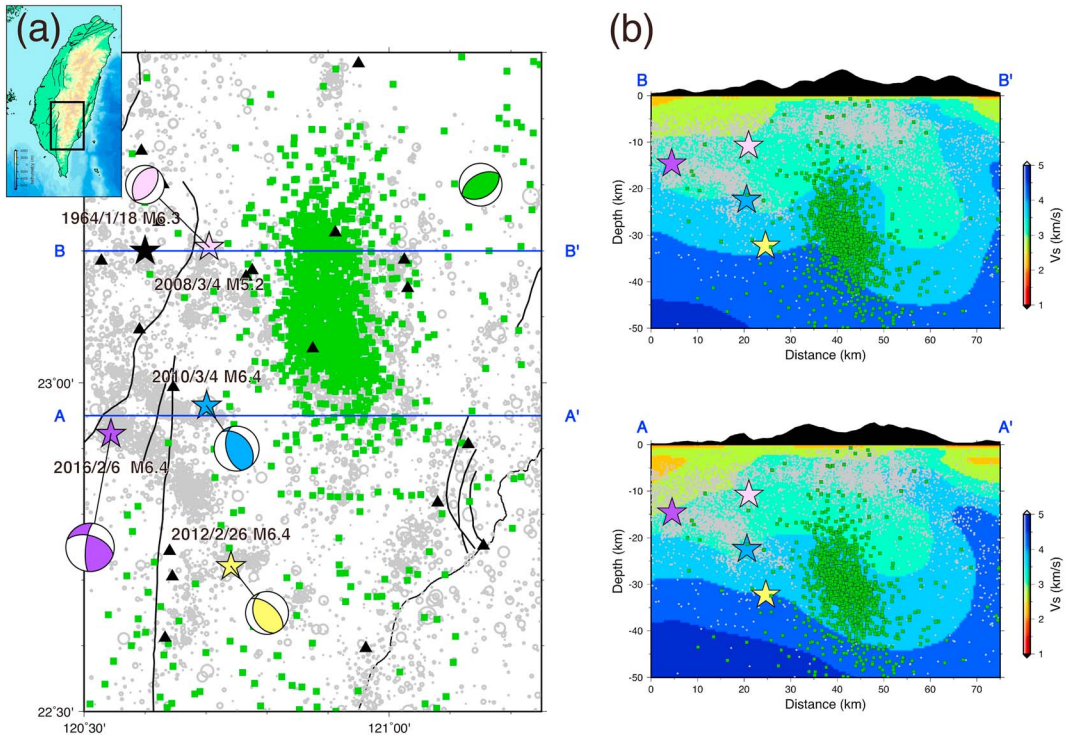

Figure 1. (a) Map of topography in Taiwan (shown in the inset) and distribution of tremors, earthquake clusters, and seismic stations used in this study. During the study period (2007–2012, 2016), four earthquake clusters with a mainshock of $M > 5$ occurred in the study area (box). The locations of these four mainshocks (the 2008/3/4 M_L 5.2 Taoyuan, 2010/3/4 M_L 6.4 Jiashian, 2012/2/26 M_L 6.4 Wutai, and 2016/2/6 M_L 6.4 Meinong earthquakes) are denoted by colored stars. The historical Baihe earthquake in 1964 is indicated by black star. The locations of tremor and background seismicity are indicated by green squares and gray circles, respectively. Black lines indicate the active faults in the study area. The faults associated with mainshock-aftershock activities are indicated by red lines. The focal mechanisms for the mainshocks are from Table 1, whereas the green beach ball for tremor is from Chen et al. (2018). Seismic stations used for tremor detection are indicated by triangles. (b) Cross-sections showing the spatial association between seismicity (gray circles) and tremors (black circles). For location of A-A′ and B-B′, please see Figure 1. Red star indicates $M > 5$ events during the study period. V_S velocity structure is from Huang et al. (2014). Dates are formatted as year/month/day.

south of the 2008 event and just 5 km east of the Chaochou fault (blue star in Figure 1). The joint source inversion from teleseismic body wave, coseismic GPS displacement, and near field ground motion data reveals a source mechanism of strike = 324°, dip = 39°, and rake = 67° (Lee et al., 2013). In 2012, the M_w 5.9 Wutai earthquake occurred to the south of the study area (yellow star in Figure 1) that is likely promoted by static stress changes of the Jiashian earthquake (Chan & Wu, 2012). The inferred NE–SW compressional stress for both the Wutai and Jiashian earthquakes rules out the contribution of the nearby north–south striking Chaochou fault. The most damaging event occurred in 2016 on 6 February, the M_w 6.3 Meinong earthquake occurred close to the epicenter of the 2010 M_w 6.4 Jiashian event (purple star in Figure 1). The shaking caused 115 deaths in Tainan City that is 35 km away from the epicenter. Such a severe hazard was unexpected and was probably linked to the shallow-thrust duplex system (5- to 10-km depth) triggered by the deep mainshock (15- to 20-km depth; Huang et al., 2016).

The four mainshocks are pure thrust faulting except for the 2016 Meinong earthquake that has more strike slip component. The mainshocks are located to the west of the tremors during the study period of 2007 to 2012 (green squares). Chan and Wu (2012) confirmed the interactive relationships between large events in this area, which is, the $M > 5.5$ events can be explained by positive stress changes promoted by the 2008 Jiashian earthquake. Down to the bottom of seismogenic zone, how does the slowly slipping area that host tremors respond to the earthquakes at shallow depths? Is a specific fault geometry needed to facilitate the interaction between slow and fast slip events? Using the 2007–2012 and 2016 tremor and earthquake catalogs in the southern Central Range, we aim to explore the relationship between tremors and major

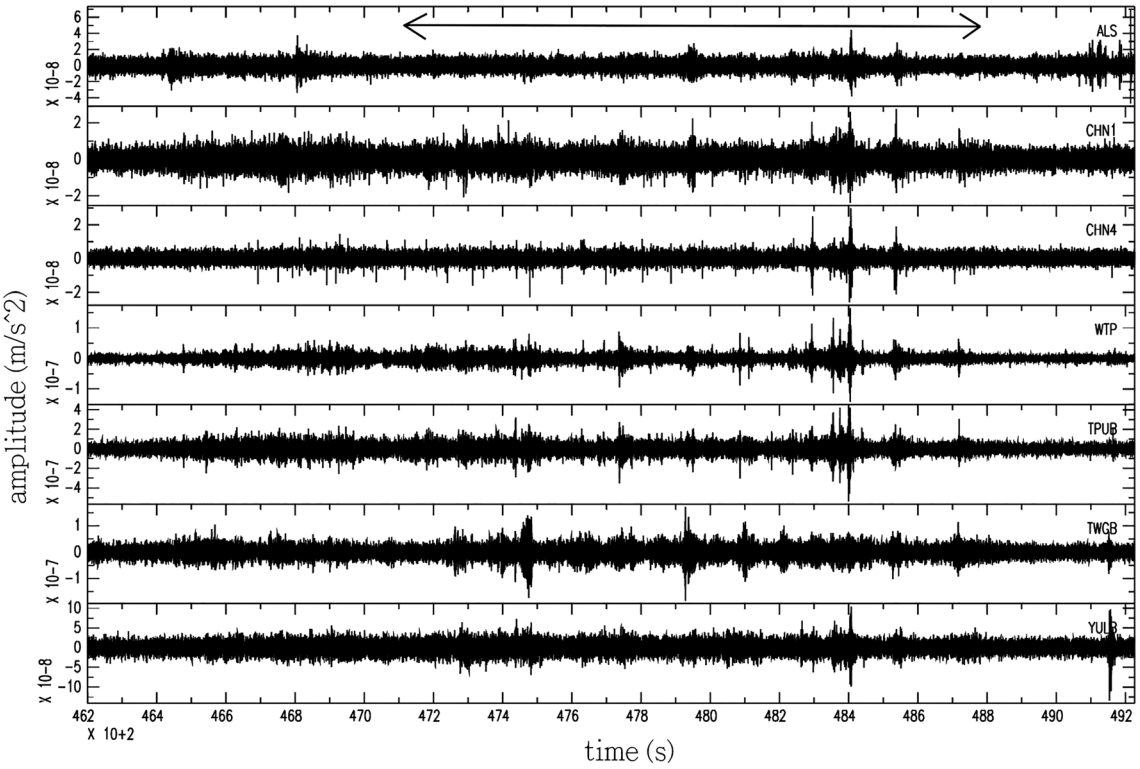

Figure 2. Example of 2–8 filtered, E-W component ambient tremor in a 26-min-long seismogram that occurred on 22 August 2008. During this selected time window, no local or teleseismic earthquakes were recorded.

earthquakes in this complex tectonic region, through examining the occurrence rate and duration of tremor activities. Further, we also study whether their spatiotemporal association can be explained by static stress triggering.

2. Catalog of Ambient Tremors and Earthquakes

The ambient tremors in this study were detected by seven broadband stations in Broadband Array in Taiwan for Seismology (BATS) and 11 short-period stations from the Central Weather Bureau Seismic Network (CWBSN) in a 6-year period (2007–2012; Chen et al., 2018). Combined with BATS, a temporary array deployed on the southern Central Range also allows us to obtain a short-term tremor catalog from 1 January to 16 September 2016. The two catalogs of tectonic tremors were identified by visual inspection after applying envelope cross-correlation approach described by Ide et al. (2015). The detailed procedures are listed below: (1) The three-component seismograms are band-pass filtered from 2 to 8 Hz, enveloped, and low-pass filtered to 2 Hz for use in the envelope cross-correlation approach described by Ide (2012) and Ide et al. (2015); (2) a 300-s moving window with a 150-s overlap is applied during cross correlation; (3) a cross-correlation coefficient higher than 0.6 for more than 10 stations and a signal-to-noise ratio of greater than 1.2 are required; (4) visual inspection is applied to exclude local and distant earthquakes. As a result, 1893 tremor events with durations ranging from 60 to 2,216 s were identified in 2007–2012, while from January to September 2016 74 tremors with duration ranging from 191 s to 771 s were cataloged (green squares in Figure 1). Figure 2 shows an example of tremor recorded at multiple stations. A data set of background earthquakes is also prepared during the same time period of the tremor catalogs. This earthquake catalog was compiled by Central Weather Bureau that contains 5,412 earthquakes with magnitudes that range from 2.0–6.4 (gray circles in Figure 1).

As detailed in Ide (2012) and Chen et al. (2018), the tremor location was determined using an envelope cross-correlation technique that obtains the time difference between stations and a velocity model by Huang et al. (2014). As a result, the tremors were mainly distributed underneath the southern Central Range that

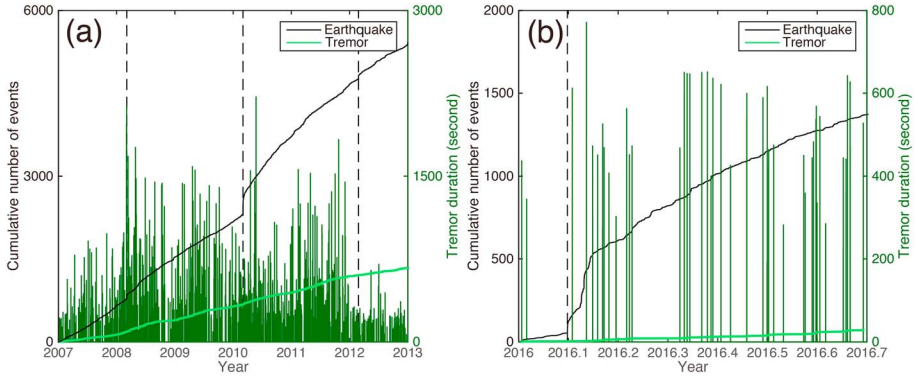

Figure 3. Cumulative number (green line) and daily duration (vertical green bar) of the tremors and $M > 2$ earthquakes (black line) using two study periods: (a) from 2007 to 2012 (b) from 2016 January to September. Vertical bars indicate the daily total duration of tremors. Vertical dashed lines indicate that the mainshocks occurred during the study period.

formed a NS-striking and SE-dipping ellipsoid structure at a depth of 20–40 km (cross-sections in Figure 1). Tectonic tremors coincide with a lower velocity zone at a depth of 15–40 km, where seismicity terminates above 15 km. West of the tremor zone (western foothills), an aseismic zone is also correlated with a lower velocity layer at a very shallow depth (below 5 km). Chen et al. (2018) explained the origin of the tremor zone as the location where continental crust of the Eurasian Plate progressively subducted, metamorphosed, and possibly detached from the subducting plate. As thicker continental crust being subducted, resisting forces along the plate boundary would likely increase, possibly leading to failure at deeper structural levels where prograde metamorphic reactions have weakened the more deeply buried rocks. The relatively high heat flow (3.2 W/m^2), high geothermal gradient (60.6 °C/km; Chi & Reed, 2008), and low seismicity in this area of Taiwan are consistent with the rapid rise of warm continental crust from deep to shallow crustal levels (Brown et al., 2015; Lin, 2002; Teng et al., 2000).

3. Elevation in Tremor Occurrence

The temporal distribution of the 1893 tremors and 5,412 earthquakes during 2007 to 2012 and 74 tremors in 2016 January to September is shown in Figure 3. We found that the longest daily duration (highest vertical bar) occurred at the time of the 2008 M_w 5.2 Taoyuan event, 46 and 13 days following the 2010 M_w 6.4 Jiashian and 2016 M_w 6.3 Meinong earthquake, respectively. The cumulative number of tremor (green line), however, reveals a constant rate instead of strong temporal variation from visual inspection. Using a sliding window analysis that determines the occurrence rate every 15 and 30 days, we obtain a short-term history of occurrence rate for tremors and earthquakes. In Figure 4, both window length reveals a clear annual variation in tremors, with two peaks coinciding to earthquake clustering in 2008 and 2010 (corresponding to the 2008 Taoyuan and the 2010 Jiashian mainshocks). The annual variation was previously interpreted by a strong tidal and seasonal modulation in Taiwan (Chen et al., 2018; Ide et al., 2015). To diminish the effect of tidal triggering that caused annual acceleration in tremor activity, we aim at removing the seasonal trend from tremor catalogs.

To do so, we applied a declustering method modified from the CURATE method (Jacobs et al., 2013) to the two tremor catalogs. This modified method reduces the arbitrary and subjective choices of space and time parameters employed in previous clustering techniques (e.g., Helmstetter & Werner, 2014; Ogata, 2011). Below we detail processing procedure: (1) Define spatial grid cell (S) and moving time window ($\underline{T}$) to select the potential cluster. In each time window T_i, earthquakes in a given grid cell S_i are connected to an adjacent grid cell if it contains more than one earthquake. (2) The connected events form a time series that starts from the event subsequent to the target event (t_{i+1}) and ends with the final event (t_e), with the cumulative earthquake total counted as N. We remove events if the interevent time is less than the average recurrence time ($t_e - t_{i+1}/N$). (3) Finalize the earthquake cluster by removing events that, because of the removal of events in the previous step, are now no longer in grid cells adjacent to those containing events. The resolution of S was set as 0.05°, according to a study on the 2007 Chuetse-oki earthquake in Japan (Peng & Toda, 2015), whereas

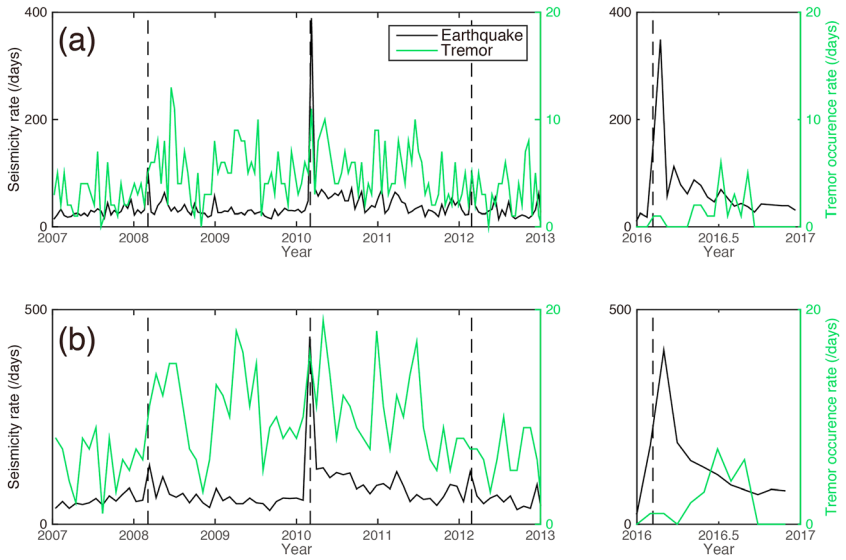

Figure 4. Short-term history of seismicitv and tremor occurrence rate that is calculated every 15 days (a) and 30 days (b). Earthquakes and tremors are indicated by black and green lines, respectively. Vertical dashed line indicates the timing of mainshocks.

T was set as 4 days based on the fact that 90% of separation times between events are confined in 4 days. Applying this clustering method to our tremor catalogs, we identified 176 tremor clusters, containing 686 events with durations of 62–2,216 s.

Using this declustered tremor catalog, we next computed β statistic values (Matthews & Reasenberg, 1988) on the two tremor catalogs. The purpose is to evaluate if the change of tremor occurrence rate is significant following the major earthquakes. Here β statistic determines changes in tremor occurrence rates by the following steps: (1) calculate the difference between the real number of events in a given time period and the expected number of events in the same time period assuming a Poisson process for the tremor occurrencel (2) normalize such difference by the standard deviation of the expected number. Using three time periods of 10, 15, and 20 days, the resulting β statistics is shown in Figures 5a and 5b. As suggested by Marsan and Wyss (2011), the efficiently significant increase of target events can be defined by β value >5. We therefore identified tremor acceleration when β values for three different sliding windows (10, 15, and 20 days) are consistently higher than 5, to ensure that the high β value remains with different selection of windows. As indicated by red line in Figure 5c where the β values from three sliding windows are summed when β values from three sliding windows are consistently higher than 5. Summation of β value from all data is also plotted for a comparison (black line in Figure 5c). The three significant accelerations (black arrows in Figure 5a and red line in Figure 5c) appear to occur 100 days after the 2008 event and at 10 and 65 days after the 2010 event. This suggests that other than the total duration of tremors following the mainshocks illustrated in Figure 3, occurrence rate of declustered tremors also reveal a possible acceleration following the 2008 and 2010 mainshocks that is worthy of attention.

4. Spatial and Temporal Association Between Tremor and Earthquakes

We further quantify the spatiotemporal association between elevated tremor activity and all earthquakes in the region. The time difference between earthquake and declustered tremor event in the catalogs (composed of 686 tremors and 5,412 earthquakes) is now computed as (1) dt+: tremor occurred prior to an earthquake (2) dt−: tremor occurred subsequent to an earthquake. Figure 6 shows the percentage of events within a given distance range that have dt− and dt+ less than 5 day, 10 days, 30 days, and 30–60 days. The wider dt range leads to greater number of events, therefore greater percentage in Figure 6. We found for |dt−| < 5 days, more percentage of tremors occurred in a short distance from earthquakes (5 km), greater than the percentage for events located further away (>10 km; dark brown in Figure 6a). To confirm that the observed short dt− population indicates the triggering effect, we compared the observed distribution with

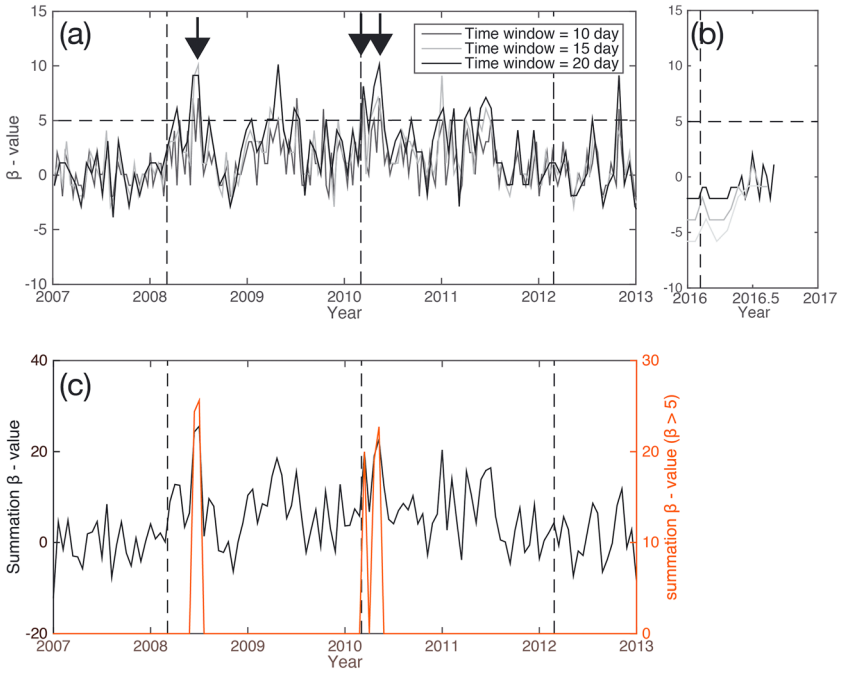

Figure 5. (a) The β value as a function of time using three different sliding windows of 10, 15, and 20 days. (b) The β value for 2016 tremor catalog. Vertical dashed lines indicate the time of four mainshocks. The black arrow denotes the time when the β value is consistently higher than 5 at three different window lengths. (c) Summation of β value from three sliding windows for all data (black line) and the data showing individual β value >5.

dt generated from randomly generated times of earthquakes. Here we generated 100 sets of synthetic catalog (541,200 events in total) by adding random noise into the declustered tremor catalogs. We kept the original catalog but randomly selected 5,412 events out of the 2,192 days where earthquakes occurred. The normally distributed random noise is chosen in a range of 365 days to a precision of four decimal places. The synthetic earthquakes produce roughly equal percentages of dt+ and dt− at varying distance, as shown by shaded lines

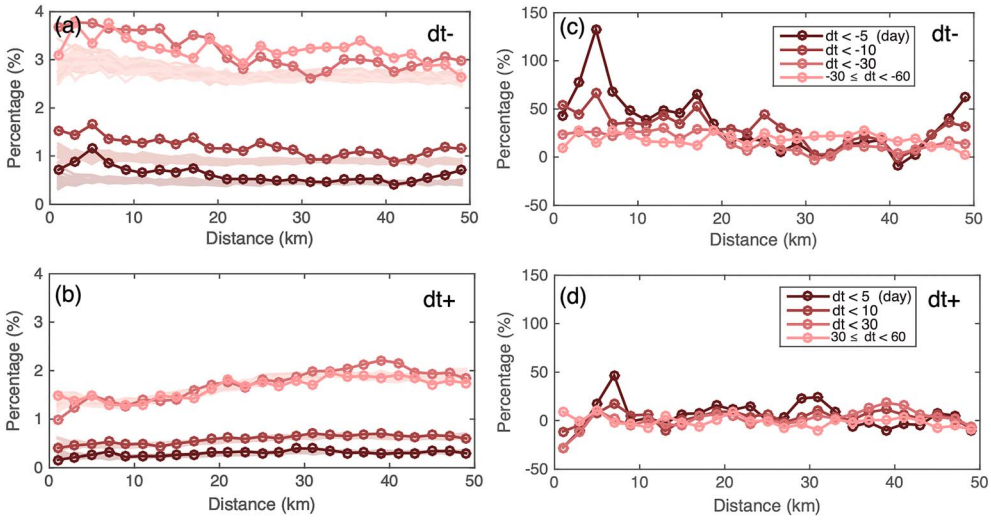

Figure 6. (a) Percentage of short dt− as a function of interevent distance between declustered tremor and earthquakes. Plotted values give percentages of events with dt− that are shorter than the label on the color-coded lines. Shaded lines indicate random behavior determined by synthetic catalogs. (b) Percentage of short dt+ as a function of distance from earthquakes. The shaded lines indicate the results from 100 sets of synthetic earthquake catalog. (c, d) Normalized percentage of (a) and (b), which is calculated by the ratio of real dt+/dt− population to the one calculated by synthetic catalogs.

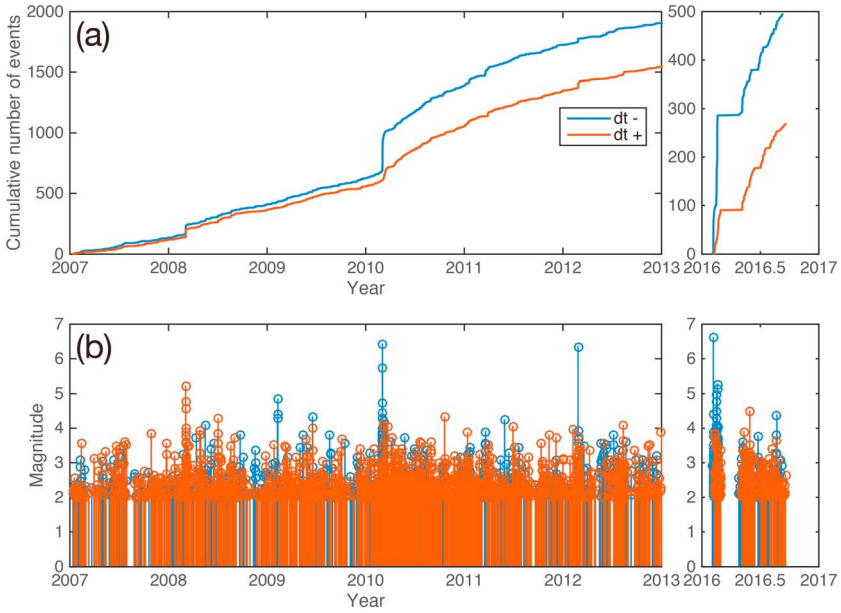

Figure 7. (a) Temporal distribution of cumulative number of earthquakes that occurred within a distance of 10 km and 5 days prior to (d*t*−) and following (d*t*+) the tremors. Bottom figure (b) shows the corresponding magnitude.

in Figure 6. The random behavior of *dt*− population is significantly different from the real population in the near field. This can be better illustrated by the ratio between the real d*t*+ and d*t*− population and the one calculated by synthetic catalogs:

$$\left(\frac{N_{\text{real}}-N_{\text{synthetic}}}{N_{\text{synthetic}}}\right)\times 100, \tag{1}$$

the N_{real} and N_{sythetic} represent the observed and synthetic number of events counted for different distance and d*t* ranges. As shown in Figure 6c, in a confined distance of 10 km, a greater percentage of earthquakes (more than 50% of the synthetic value) tend to occur in 5 days prior to the tremors. Compared to d*t*− curves, short d*t*+ population does not reveal systematic changes with distance, as the short d*t*+population remains the same with random behavior (shaded lines) over distance in Figure 6b and a constant percentage in Figure 6d except for d*t*+ < 5 days and distance shorter than 10 km. The contrast, although minor, suggests that the near-field triggering of tremor responsible for d*t*− population is more significant and possible. Within 10 km, the relatively greater d*t*− population reveals close association between tremor and earthquakes, which cannot be explained by random chance. The earthquakes responsible for the spike in Figures 6c and 6d (d*t* < 5 days and separation distance <10 km) are found to be clustered at the time of the 2010 and 2016 mainshocks, as revealed by the elevation of occurrence rate and magnitude distribution in Figure 7, though the number of earthquakes may not be statistically sufficient for the year of 2016. The role of magnitude is confirmed in the plot of the normalized percentage versus event magnitude in Figure 8. For greater magnitude ($M > 5$), more percentage of tremors tends to occur in a short time following the earthquakes (|d*t*−| < 5 days). The combined effect of magnitude and distance can be further considered by the calculation of static stress change. In the following sections we will address Coulomb stress change induced by (1) four mainshocks and (2) all earthquakes in the catalog, to understand whether such temporal association can be explained by static stress triggering.

5. Coulomb Stress Change Induced by Four Mainshocks

The coseismic slip models for 2008 Taoyuan, 2010 Jiashian, 2012 Wutai, and 2016 Meinong mainshocks were derived from Shih et al. (2014), Lee et al. (2013), Chiang et al. (2016), and Huang et al. (2016), respectively. The fault parameters corresponding to each of the mainshocks are listed in Table 1. Due to the large

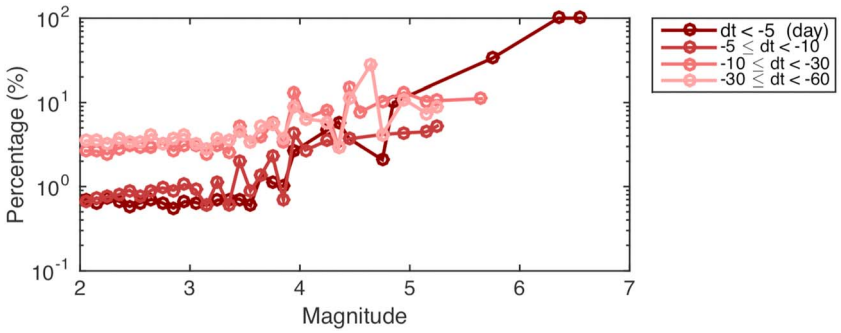

Figure 8. Normalized percentage of dt- as a function of magnitude. The normalized percentage is the ratio of real dt- population to the one calculated by synthetic catalog.

location uncertainty and the weak signals for tremor events (Chen et al., 2018), the slip model for tremors was less certain. We used the empirical relationship between tremor duration and GPS-derived seismic moment by Aguiar et al. (2009), to approximate the moment magnitude of tremor. It should be noted that the inferred regression line in Aguiar et al. (2009) is derived from the tremors and slow slip events in Cascadia. In our study area where the tremors tend to shorter than 30 min and slow slip event is not resolvable on geodetic measurements, it is difficult to examine the tremor versus slow slip relationship. Thus, we simply assume that there exists a universal rule between tremor duration and GPS-derived seismic moment. The observed tremor with longest duration (36.9 min) gives the tremor magnitude of M_w 4.9. The fault orientation for tremor events was considered as a low-angle thrust (strike = N54°E, dip = 13°, rake = 120°), derived from a moment tensor inversion based on very low frequency events (Ide et al., 2015). Using a more complete tremor catalog, Chen et al. (2018) obtained a slightly different fault orientation (strike = N60°E, dip = 40°, rake = 90°), which also reveals a strong correlation with the tides. Since we used the same tremor catalog as Chen et al. (2018), the fault orientation of strike = N60°E, dip = 40°, rake = 90° is chosen for our static Coulomb stress computation.

As illustrated in Figure 9, the 2008 Taoyuan, 2010 Jiashian, and 2016 Meinong earthquakes produced a Coulomb stress change of 0.2, 8, and 0.2 kPa, respectively, averaged along the low-angle thrust tremor zone at a depth of 30 km. The 2012 Wutai earthquake, however, produced negative stress changes in the tremor zone of −0.3 kPa. The sign of stress changes could change with fault orientation and depth of receiver (tremor source). A series of sensitivity tests, therefore, was conducted to illustrate how the Coulomb stress change alters with the tremor depth, strike, dip, and rake of the tremor zone.

In Figures 10 and 11, we found that under different combinations of strike, dip, rake, and depth, Coulomb stress change induced by the 2008 Taoyuan and 2012 Wutai earthquakes are extremely small, <1 kPa. Moreover, Coulomb stress change is very sensitive to receiver depth. When the tremor is placed at 30-km depth, 96%, 72%, 25%, and 86% of data points show positive stress change for the Taoyuan, Jiashian, Wutai, and Meinong earthquakes, respectively. With increasing receiver depth to 40 and 50 km, much less percentage of data points coincides with positive stress change. To have positive stress changes been observed at different depths for the 2008 Taoyuan earthquake, the necessary dip and rake is in a range of 50–90° and 20–30°, respectively (colored circles in Figures 10b and 10c); however, no certain strike range allows for consistent positive stress change over depth (Figure 10a). For the 2010 Jiashian earthquake, there exists a wide range of strike, dip, and rake for positive stress change (Figures 10d–10f), supporting the

Table 1
Fault Parameters for Coseismic Slip Models Used in This Study

	Mainshock location (lon, lat, depth)	Magnitude (*Mw*)	Fault length (km)	Fault width (km)	Max. slip (m)	Average slip (m)	Average rake (°)	Average dip (°)	Reference
Taoyuan	(120.70, 23.20, 10.8)	5.2	18	10	0.0052	0.0052	96	48	Shih et al. (2014)
Jiashian	(120.70, 22.96, 22.4)	6.4	42	48	0.27	0.052	39	39	Lee et al. (2013)
Wutai	(120.74, 22,72, 32)	5.9	30	15	0.09	0.065	49	30	Chiang et al. (2016)
Meinong	(120.42, 22.95, 22.9)	6.3	45	40	0.73	0.12	27	17	Huang et al. (2016)

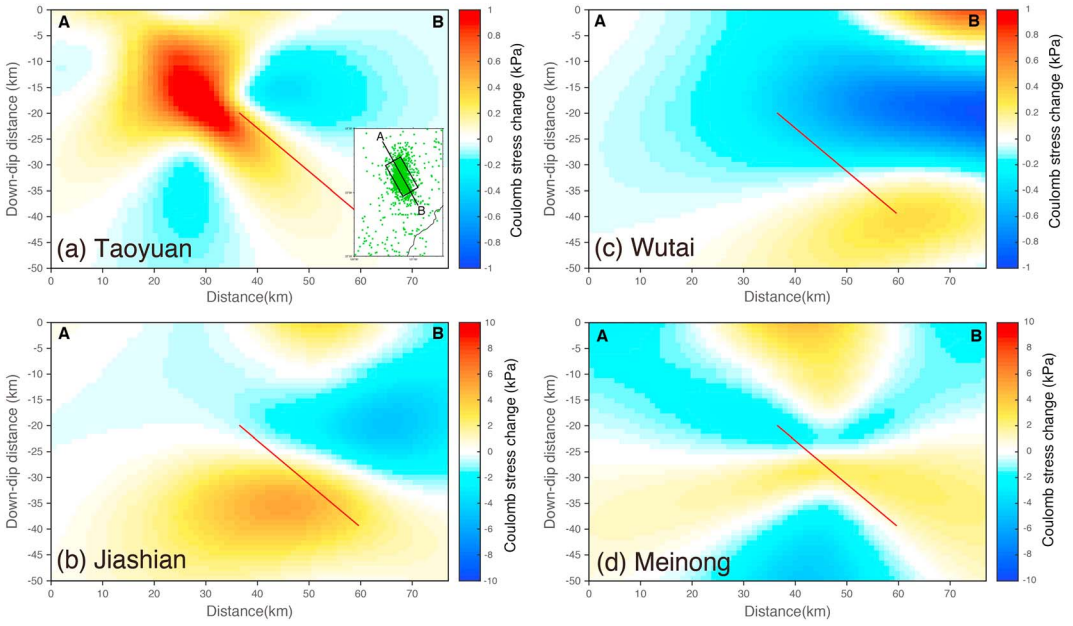

Figure 9. Static Coulomb stress change caused by the (a) 2008 Taoyuan, (b) 2010 Jiashian, (c) 2012 Wutai, and (d) 2016 Meinong events on tremor source, along the cross-section A-B (shown in inset of a). Here we assume a receiver depth of 30 km (horizontal dashed line) and fault plane (red line) corresponding to the best correlation with tidal stress by Chen et al. (2018).

triggering relationship between mainshock and tremors earlier seen in Figures 6 and 7. For the 2012 Wutai earthquake, despite the strike = 160–210° and the rake = 110–180° reveal positive stress change, no certain dip range is able to produce positive stress change (Figures 11a–11c). Similarly for the 2016 Meinong earthquake, only a limited range of strike (300–340°) allows for positive stress change at various depths (Figures 11d–11f). The fault orientation of strike = N54°E, dip = 13°, rake = 120° inferred by Ide et al. (2015) reveals the same result. This suggests that (1) only the 2010 Jaishian event was able to produce sufficient and consistent stress perturbation that promotes the tremor activity under a variety of receiver geometry and depth; (2) if the positive correlation of tremor activity with the 2010 mainshock is explained by static stress triggering, the fault orientation for the tremor structure must have been a thrust faulting with a minor right-lateral component.

6. Coulomb Stress Change Induced by All Earthquakes

We also examine the effect from smaller earthquakes by conducting a 3-D event interaction model based on isotropic, elastic half-space dislocation solutions. Normal, shear, and Coulomb stress changes were calculated on the tremor source. With the location from the relocated earthquake catalog by Wu et al. (2008), we discretized a circular rupture patch into many small rectangular elements and impose an elliptical slip distribution to ensure a uniform stress drop 3 MPa. The rupture area (A) of the circular slip patch is derived using Hanks-Bakun scaling $A = 10^{(\mathrm{Mw}-3.98)}$ (Hanks & Bakun, 2008) and the mean slip (D) over the patch is $D = M_0/(\mu A)$ where μ is the shear modulus. We utilized data sets of background earthquakes from 2007 to 2012 compiled by Central Weather Bureau. In our computation, an earthquake that occurred closest to tremor in time, is regarded as a single source. All source events are assumed to have a faulting mechanism that is the same with the averaged strike, dip, and rake from the representative events. Since the focal mechanism for the 2008 Taoyuan earthquake is different from the rest of three mainshocks, here we consider two different fault orientation for source events (see Figures 12a and 12b). The stress change from 1967 sources (1893 in the 2007–2012 catalog and 74 in the 2016 catalog) are computed on tremor zone of strike = N60°E, dip = 40°, rake = 90°. The resulting Coulomb stress change at the time of each tremor is shown by curves in Figure 12, where the stress change produced by seismicity is only a few pascals, with ~60% tremors occurring under positive stress changes from preceding earthquakes. While there is no example in the literatures for

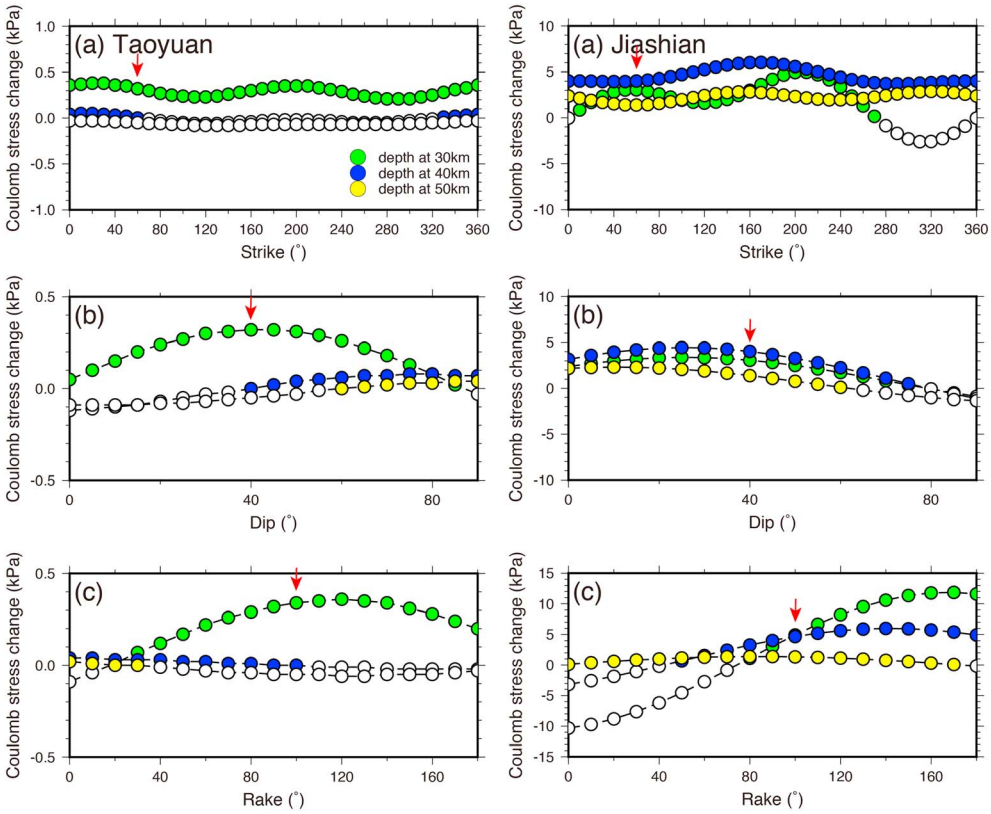

Figure 10. Coulomb stress change induced by the (left column) 2008 Taoyuan and (right column) 2010 Jiashian earthquakes a function of the strike, dip, and rake of the receiver (tremor). In (a), the assumed dip = 40° and rake = 90°; in (b), the assumed strike = N60°E and rake = 90°; in (c), the assumed strike = N60°E and dip = 40°. The filled circles indicate the positive Coulomb stress change. Red arrow indicates the preferred fault orientation by Chen et al. (2018).

supporting static stress triggering at such small number (a few pascals), we concluded no strong evidence of triggering between tremors and preceding small earthquakes (magnitude ranging from 2.0 to 4.1) in this study.

7. Physical Condition Sensitive to Small Stress Change

In contrast to subduction zones, tremors observed at the San Andreas fault in the United States, the Alpine fault in New Zealand, and the thrust-faulting structure in Taiwan are characterized by shorter durations, usually tens of minutes (Chuang et al., 2014; Nadeau & Guilhem, 2009; Wech et al., 2012). Like the tremor-earthquake interactions discovered here, tremor activity at Parkfield is found to be accelerated for several years following two strong earthquakes (Nadeau & Guilhem, 2009). Such close associations are not seen in the worldwide subduction zones, where longer tremors (hours to days) occur. The stress change induced by coseismic slip is several kilopascals in Parkfield (Nadeau & Guilhem, 2009) and <1 kPa in this study, which is similar to the stress change induced by tidal forcing (e.g., Ide, 2010), As proposed by Ide (2010, 2012), tremor duration appears to be negatively correlated with sensitivity to tidal stress, which can be explained by a quick pickup and termination of external load in a small tremor patch surrounded by numerous brittle patches. Longer tremors, on the other hand, located around less-dense brittle patches, are expected to experience a longer diffusional slip migration, which is less influenced by tidal stress. In places where tremor duration is short, could be as sensitive to small stress changes induced by major earthquakes in the vicinity.

Tremors in Taiwan were found to be triggered by teleseismic surface waves, where the threshold of dynamic stress triggering is determined as 7–8 kPa (Chao et al., 2012; Peng & Chao, 2008). The computation of theoretical tidal stress using the sum of the ocean and solid Earth tides by Ide et al. (2015) shows that the tremors

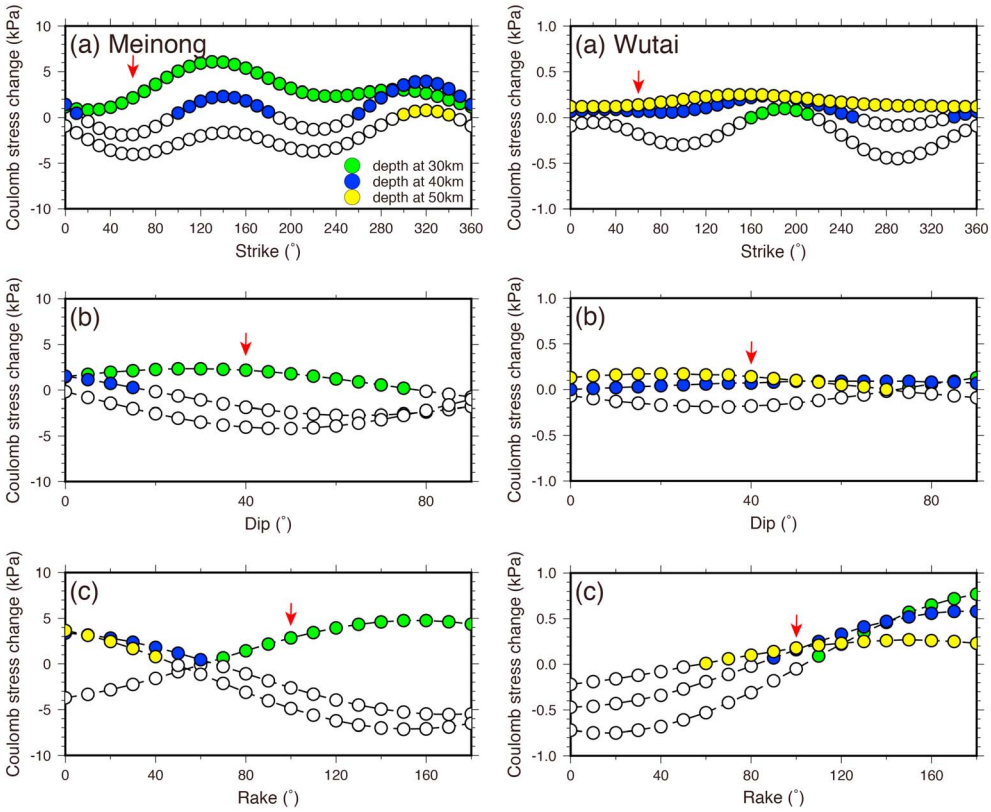

Figure 11. Coulomb stress change induced by the (left column) 2012 Wutai and (right column) 2016 Meinong earthquakes a function of the strike, dip, and rake of the receiver (tremor). In (a), the assumed dip = 40° and rake = 90°; in (b), the assumed strike = N60°E and rake = 90°; in (c), the assumed strike = N60°E and dip = 40°. The filled circles indicate the positive Coulomb stress change. Red arrow indicates the preferred fault orientation by Chen et al. (2018).

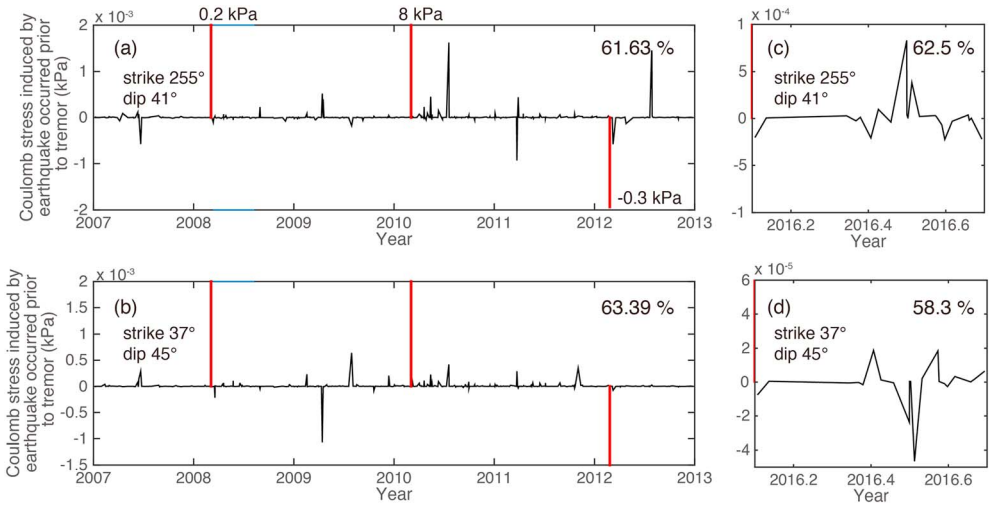

Figure 12. Time evolution of Coulomb stress change using 3-D dislocation model assuming sources have the same fault geometry. The fault orientation is derived from (a) averaged value from the 2010, 2012, and 2016 mainshocks that have similar focal mechanisms (see Figure 1) and (b) the 2008 Meinong mainshock. Panels (c) and (d) are for 2016 tremor catalog. Red line indicates the sign of Coulomb stress change computed using coseismic slip model, which the resulting Coulomb stress changes are 0.2, 8, 0.3, and 0.2 kPa, respectively.

tend to occur when tidal shear stress is positive and normal stress is negative. Such strong modulation of tidal stress produces shear stress of ~1 kPa, which is smaller than the Jiashian mainshock-induced shear stress (several kilopascals in average). Triggering of tremors by very small stress perturbation may happen under specific conditions such as (1) when fault is critically stressed, (2) when fault resistance is greatly reduced by an increase in pore fluid pressures, (2) when stress change from poroelastic deformation is sufficiently large, or (3) both mainshock and tremor activities are driven by common mechanisms (e.g., slow slip and aseismic deformation transients; Bürgmann, 2018; Obara & Kato, 2016; Rubinstein et al., 2009; Schwartz, 2015; Shelly et al., 2011). Here we favor the second and third conditions based on the unique tectonic setting of the tremor zone in Taiwan. The reason is, from Coulomb failure criterion below, the stress (τ as shear stress and σ_n as normal stress) and fluid pressure (P_f) on a fault plane affects its stability:

$$\tau = c + \mu_s(\sigma_n - P_f), \tag{2}$$

where c is the intrinsic cohesion of the fault and μ_s is the static coefficient of friction. When P_f increases with constant τ and σ_n, the fault failure could occur more easily. In a thickening crust that undergoes prograde metamorphic dewatering, the overpressure fluid plays an important role in fault failure that leads to reverse-slip rupturing in middle to lower crust (Sibson, 2009). The high-fluid pressure may potentially control recurrence of earthquake ruptures (Sibson & Rowland, 2003).

Tectonic tremors underneath the southern Central Range of Taiwan are located in a low-velocity zone at a depth of 15–40 km, where seismicity terminates above 15 km (cross-sections A and B in Figure 13). The number of tremors decreases dramatically when the velocity increases (cross-section C). An aseismic zone (zone W) with a lower velocity appears to the west of the tremor area at a very shallow depth (below 5 km), forming an east dipping slope that connects with the downdip tremor zone (zone M). The deeper zone M is characterized by high heat flow (Chi & Reed, 2008), low resistivity (Bertrand et al., 2012; Chiang et al., 2010), low Q value (Lee et al., 2010; Wang et al., 2010), and a low-V, high Poisson's ratio (Toyokuni et al., 2016), suggesting a geothermal anomaly with 0.4–1.4% fluid content (Bertrand et al., 2012) in the middle to lower crust. The low-velocity zone W is also characterized by high heat flow (Hsieh et al., 2014), low magnetotelluric resistivity (Bertrand et al., 2012), high Poisson's ratio (Toyokuni et al., 2016), and ~2.0 V_p/V_s ratio (Huang et al., 2014), suggesting an abnormally high fluid pressure zone at shallow depths. Comparing these two zones, their common characteristics (high heat flow, low resistivity, and low-V, high-Poisson's ratio) may explain the seismic gap and the sparse seismicity along the path from M to W. Such fluid-rich bodies are probably the result of active prograde metamorphism at a greater depth ascending to the shallow crust. The slope connecting M to W likely indicates a structure that was formed when the crustal slices started to uplift during continental subduction. This structural connection between a shallow thrust duplex system (Huang et al., 2016) and a thrust fault that roots into lower crust may be needed to explain the 1–2 cm/year interseismic surface uplift rate (Ching et al., 2011) measured across Central Range from zone M to zone W (specifically the west of the Meinong event hypocenter). The combination of changes in stress and fluid pressure level could play a role in the triggering relationship between tremors and earthquakes in this area. A structural connection between M and W may exist, as denoted by the white lines in Figure 13, which allows the poroelastic stress transfer induced by fluid flow to happen. As the static poroelastic stress transfer being accumulated during slow aseismic slip events (Rogers & Dragert, 2003), the interaction with fast-slip phenomena along the pathway could be facilitated. The poroelastic processes that cause pressure and strain accumulations is difficult to characterize, therefore, could be the missing source of stress change in our stress computation.

8. Uncertainties in Stress Computation

If the stress interaction between tremor and mainshocks exist, should the negative static stress change induced by the 2012 mainshock suggest a decrease of tremor rate? We found that the tremor activity reveals no declined pattern in Figures 3 and 4. The paucity of the shadow effect may come from (1) uncertainty in fault parameters for mainshocks, (2) uncertainty in fault plane solution for tremors, and (3) the role of static stress change in the triggering relationship. Among the four mainshocks, the slip models were inferred from GPS and/or seismic data except for the 2008 M 5.2 Taoyuan mainshock. The rupture length (RLD) and width

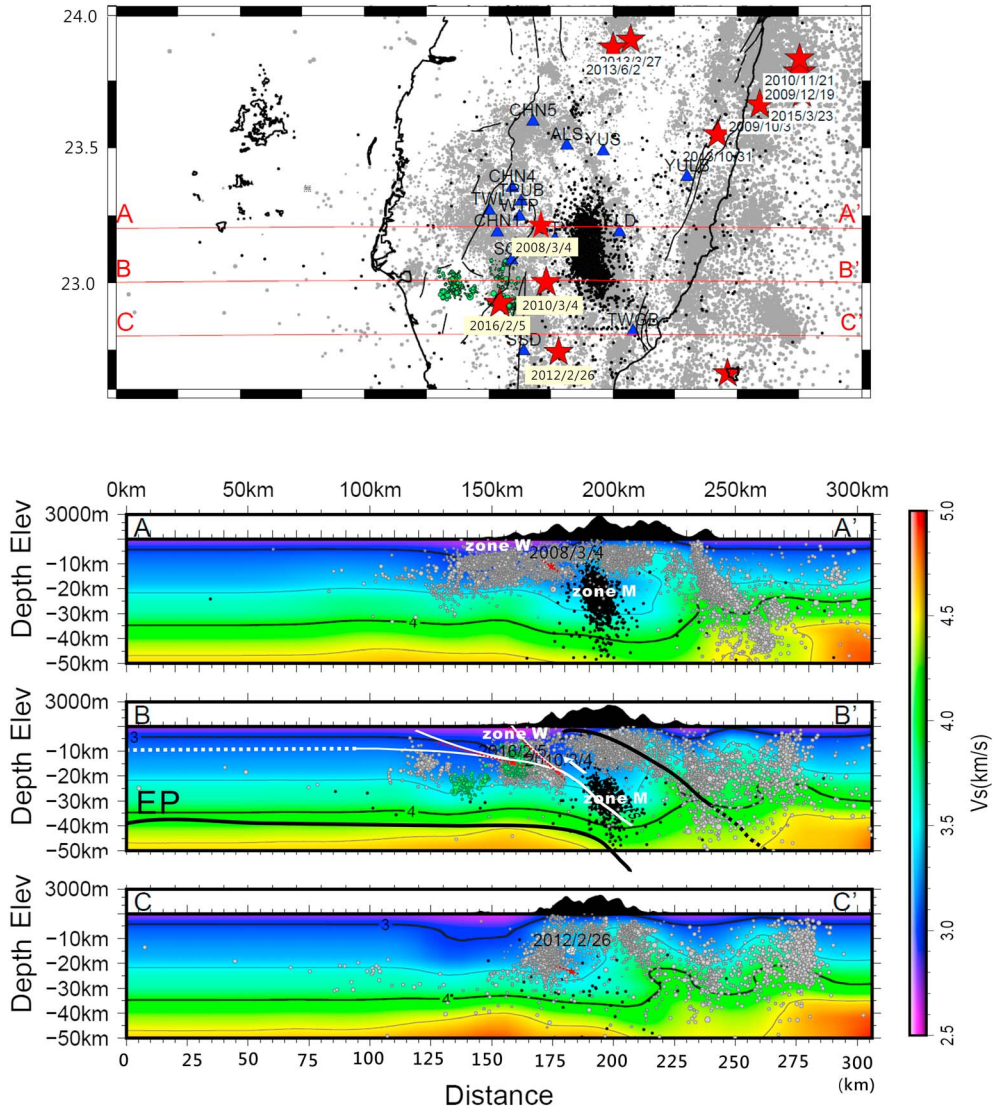

Figure 13. Map and cross sections showing the spatial association between tremors (black circles) and mainshocks (red stars). Background seismicity is denoted by gray circles. Green circles represent the aftershock of the most recent *M*6.4 Meinong event. Red dashed lines in the cross-sections indicate the fault models assumed in the Coulomb stress computation in this study. Black and white lines in cross-section B show a conceptual model for a plate boundary and structural connection between the tremor zone and mainshocks. Tomographic images are from Huang et al. (2014).

(RW) for this 2008 event was determined using equations below, in order to infer the slip magnitude as slip offset = Mo/(shear modulus × RLD × RW).

$$\text{Log RLD} = -2.42 + 0.58\,M_w \quad \text{(Wells \& Coppersmith, 1994)} \tag{3}$$

$$\text{Log RW} = -1.61 + 0.41\,M_w \quad \text{(Wells \& Coppersmith, 1994)} \tag{4}$$

$$\log M_o = 1.5M_w + 16.095 \quad \text{(Hanks \& Kanamori, 1979)} \tag{5}$$

The uniform and oversimplified slip inferred using empirical relationships in the 2008 event may lead to a biased result and interpretation, while three other source models also have uncertainties that propagate through the Coulomb stress calculations (e.g., Parsons, 2004). In this study we did not test the stress computation using different source models, given the selected models themselves were compared with other results in the original papers (Chiang et al., 2016; Huang et al., 2016; Lee et al., 2013; Shih et al., 2014). Instead, we

attempted to approach uncertainty produced by receiver fault orientations, as shown in Figures 10 and 11. The depth, strike, dip, and rake are found to be very sensitive to the sign of Coulomb stress change especially when the magnitude of stress change is small.

The lack of resolvable decreases in seismicity rate could be that earthquake triggering is dominated by the dynamic stresses (Felzer et al., 2004; Felzer & Brodsky, 2005). For example, a weak correlation between small intraslab earthquakes and tremors was explored in southwest Japan, where the triggering of tremor by earthquakes tends to be more significant than triggering of earthquakes by tremor (Han et al., 2014). Such different triggering potential, as they interpreted, is from the larger dynamic stress changes induced by earthquakes. Given the near-field dynamic stress triggering is difficult to be discriminated from static stress triggering, we cannot rule out the role of dynamic processes in the tremor-earthquake interaction in the study area. As previously discovered in Ide et al. (2015) and Chen et al. (2018), the role of tidal stress modulation in tremor activity is also possible, given the magnitude (several kilopascals) is similar with the coseismic slip induced stress change. What this study performed is the statistically significant correlation between the increased tremor rate in 2010, where the static stress triggering may play an important role in their interaction.

9. Conclusion

On 6 February 2016, the M_w 6.3 Meinong earthquake occurred in southern Taiwan. The strong shaking caused 115 deaths in Tainan City, 35 km away. Apart from this recent event, several other mainshocks have struck the same area: the 4 March 2008 M_w 5.2 Taoyuan earthquake, the 4 March 2010 M_w 6.4 Jiashian earthquake, and the 26 February 2012 M_w 5.9 Wutai earthquake. By examining the rate of occurrence and duration of tremor activity, we have explored the relationship between tremors and major earthquakes in this study area. Using β statistics on the 2007–2012 and 2016 earthquake and declustered tremor catalogs, we found that tremors increased near the time of the 2008 M_L 5.2 Taoyuan and 2010 M_L 6.4 Jiashian earthquakes, whereas in 2012 and 2016 the tremors showed no significant response to the large earthquake. When the spatiotemporal association between elevated tremor activity and earthquakes are further quantified using time difference between earthquake and declustered tremor event, we found an evidence of short-term triggering. In a confined distance of 10 km, a greater percentage of earthquakes tend to occur in 5 days prior to the tremors. The 2010 Jiashian earthquake appears to be most responsible for such signature of short-term triggering.

With a low dip angle thrust faulting in the tremors, calculation of the static Coulomb stress change further showed that the tremors were located in areas of enhanced static stress change induced by the 2010 mainshocks. The 2008 Taoyuan, 2012 Wutai, and 2016 Meinong events, however, caused either extremely small positive stress change (<1 kPa) or negative stress change in the tremor zone. These findings suggest that the different responses of tremors can be explained by coseismic slip-induced static stress change. The deeper tremor zone and areas above the mainshocks, both characterized by anomalously high temperature gradients, low velocity, high Poisson's ratio, and low resistivity, share a common mechanism for the seismic gaps. In this hot, fluid-rich environment with a possible structural connection between tremors and earthquakes, stress triggering could occur with small stress changes of several kPa.

Acknowledgments
We are grateful to Tim Byrne for helpful discussion on the tectonic interpretation on the tremor generation. We thank Willy Yen for providing the 2016 tremor catalog. Figures were made with GMT (Wessel & Smith, 1995). Support for this work was provided by MOST grant 103-2116-M-003-001-MY5. Seismic data are archived at the Central Weather Bureau Seismic Network (http://gdms.cwb.gov.tw/index.php) and the Broadband Array in Taiwan for Seismology operated by IES (http://bats.earth.sinica.edu.tw/Data/index.html).

References

Aguiar, A. C., Melbourne, T. I., & Scrivner, C. W. (2009). Moment release rate of Cascadia tremor constrained by GPS. *Journal of Geophysical Research*, *114*, B00A05. https://doi.org/10.1029/2008JB005909

Bertrand, E. A., Unsworth, M. J., Chiang, C.-W., Chen, C.-S., Chen, C.-C., Wu, F. T., et al. (2012). Magnetotelluric imaging beneath the Taiwan orogen: An arc-continent collision. *Journal of Geophysical Research*, *117*, B01402. https://doi.org/10.1029/2011JB008688

Brown, J. R., Beroza, G. C., Ide, S., Ohta, K., Shelly, D. R., Schwartz, S. Y., et al. (2009). Deep low-frequency earthquakes in tremor localize to the plate interface in multiple subduction zones. *Geophysical Research Letters*, *36*, L19306. https://doi.org/10.1029/2009GL040027

Brown, L., Wang, K., & Sun, T. (2015). Static stress drop in the M_w 9 Tohoku-oki earthquake: Heterogeneous distribution and low average value. *Geophysical Research Letters*, *42*, 10,595–10,600. https://doi.org/10.1002/2015GL066361

Brudzinski, M. R., Hinojosa-Prieto, H. R., Schlanser, K. M., Cabral-Cano, E., Arciniega-Ceballos, A., Diaz-Molina, O., & DeMets, C. (2010). Nonvolcanic tremor along the Oaxaca segment of the middle America subduction zone. *Journal of Geophysical Research*, *115*, B00A23. https://doi.org/10.1029/2008JB006061

Bürgmann, R. (2018). The geophysics, geology and mechanics of slow fault slip. *Earth and Planetary Science Letters*, *495*, 112–134. https://doi.org/10.1016/j.epsl.2018.04.062

Chan, C.-H., & Wu, Y.-M. (2012). A seismicity burst following the 2010 *M* 6.4 Jiashian earthquake—Implications for short-term seismic hazards in southern Taiwan. *Journal of Asian Earth Sciences*, *59*, 231–239. https://doi.org/10.1016/j.jseaes.2012.08.011

Chao, K., Peng, Z., Wu, C., Tang, C.-C., & Lin, C.-H. (2012). Remote triggering of non-volcanic tremor around Taiwan. *Geophysical Journal International*, *188*(1), 301–324. https://doi.org/10.1111/j.1365-246X.2011.05261.x

Chen, K. H., Tai, H.-J., Ide, S., Byrne, T. B., & Johnson, C. W. (2018). Tidal modulation and tectonic implications of tremors in Taiwan. *Journal of Geophysical Research: Solid Earth*, *123*, 5945–5964. https://doi.org/10.1029/2018JB015663

Chi, W.-C., & Reed, D. L. (2008). Evolution of shallow, crustal thermal structure from subduction to collision: An example from Taiwan. *Geological Society of America Bulletin*, *120*(5–6), 679–690. https://doi.org/10.1130/B26210.1

Chiang, C.-W., Chen, C.-C., Unsworth, M., Bertrand, E., Chow-Son, C., Kieu, T. D., & Hsu, H.-L. (2010). The deep electrical structure of southern Taiwan and its tectonic implications. *TAO: Terrestrial, Atmospheric and Oceanic Sciences*, *21*(6), 8. https://doi.org/10.3319/TAO.2010.02.25.01(T)

Chiang, P.-H., Hsu, Y.-J., & Chang, W.-L. (2016). Fault modeling of the 2012 Wutai, Taiwan earthquake and its tectonic implications. *Tectonophysics*, *666*, 66–75. https://doi.org/10.1016/j.tecto.2015.10.015

Ching, K.-E., Johnson, K. M., Rau, R.-J., Chuang, R. Y., Kuo, L.-C., & Leu, P.-L. (2011). Inferred fault geometry and slip distribution of the 2010 Jiashian, Taiwan, earthquake is consistent with a thick-skinned deformation model. *Earth and Planetary Science Letters*, *301*(1–2), 78–86. https://doi.org/10.1016/j.epsl.2010.10.021

Chuang, L. Y., Chen, K. H., Wech, A., Byrne, T., & Peng, W. (2014). Ambient tremors in a collisional orogenic belt. *Geophysical Research Letters*, *41*, 1485–1491. https://doi.org/10.1002/2014GL059476

Felzer, K. R., Abercrombie, R. E., & Ekström, G. (2004). A common origin for aftershocks, foreshocks, and multiplets. *Bulletin of the Seismological Society of America*, *94*(1), 88–98. https://doi.org/10.1785/0120030069

Felzer, K. R., & Brodsky, E. E. (2005). Testing the stress shadow hypothesis. *Journal of Geophysical Research*, *110*, B05S09. https://doi.org/10.1029/2004JB003277

Han, J., Vidale, J. E., Houston, H., Chao, K., & Obara, K. (2014). Triggering of tremor and inferred slow slip by small earthquakes at the Nankai subduction zone in Southwest Japan. *Geophysical Research Letters*, *41*, 8053–8060. https://doi.org/10.1002/2014GL061898

Hanks, T. C., & Bakun, W. H. (2008). M-log A observations for recent large earthquakes. *Bulletin of the Seismological Society of America*, *98*(1), 490–494. https://doi.org/10.1785/0120070174

Hanks, T. C., & Kanamori, H. (1979). A moment magnitude scale. *Journal of Geophysical Research*, *84*(B5), 2348–2350. https://doi.org/10.1029/JB084iB05p02348

Helmstetter, A., & Werner, M. J. (2014). Adaptive smoothing of seismicity in time, space, and magnitude for time-dependent earthquake forecasts for California. *Bulletin of the Seismological Society of America*, *104*(2), 809–822. https://doi.org/10.1785/0120130105

Hsieh, H.-H., Chen, C.-H., Lin, P.-Y., & Yen, H.-Y. (2014). Curie point depth from spectral analysis of magnetic data in Taiwan. *Journal of Asian Earth Sciences*, *90*, 26–33. https://doi.org/10.1016/j.jseaes.2014.04.007

Huang, H.-H., Wu, Y.-M., Song, X., Chang, C.-H., Lee, S.-J., Chang, T.-M., & Hsieh, H.-H. (2014). Joint V_p and V_s tomography of Taiwan: Implications for subduction-collision orogeny. *Earth and Planetary Science Letters*, *392*, 177–191. https://doi.org/10.1016/j.epsl.2014.02.026

Huang, M.-H., Tung, H., Fielding, E. J., Huang, H.-H., Liang, C., Huang, C., & Hu, J.-C. (2016). Multiple fault slip triggered above the 2016 M_w 6.4 MeiNong earthquake in Taiwan. *Geophysical Research Letters*, *43*, 7459–7467. https://doi.org/10.1002/2016GL069351

Hutchison, A. A., & Ghosh, A. (2017). Ambient tectonic tremor in the San Jacinto fault, near the Anza gap, detected by multiple mini seismic arrays ambient tectonic tremor in the San Jacinto fault, near the Anza gap, detected by multiple mini seismic arrays. *Bulletin of the Seismological Society of America*, *107*(5), 1985–1993. https://doi.org/10.1785/0120160385

Ide, S. (2010). Striations, duration, migration and tidal response in deep tremor. *Nature*, *466*(7304), 356–359. https://doi.org/10.1038/nature09251

Ide, S. (2012). Variety and spatial heterogeneity of tectonic tremor worldwide. *Journal of Geophysical Research*, *117*, B03302. https://doi.org/10.1029/2011JB008840

Ide, S., Shelly, D. R., & Beroza, G. C. (2007). Mechanism of deep low frequency earthquakes: Further evidence that deep non-volcanic tremor is generated by shear slip on the plate interface. *Geophysical Research Letters*, *34*, L03308. https://doi.org/10.1029/2006GL028890

Ide, S., Yabe, S., Tai, H.-J., & Chen, K. H. (2015). Thrust-type focal mechanisms of tectonic tremors in Taiwan: Evidence of subduction. *Geophysical Research Letters*, *42*, 3248–3256. https://doi.org/10.1002/2015GL063794

Jacobs, K. M., Smith, E. G., Savage, M. K., & Zhuang, J. (2013). Cumulative rate analysis (CURATE): A clustering algorithm for swarm dominated catalogs. *Journal of Geophysical Research: Solid Earth*, *118*, 553–569. https://doi.org/10.1029/2012JB009222

La Rocca, M., Creager, K. C., Galluzzo, D., Malone, S., Vidale, J. E., Sweet, J. R., & Wech, A. G. (2009). Cascadia tremor located near plate interface constrained by *S* minus *P* wave times. *Science*, *323*(5914), 620–623. https://doi.org/10.1126/science.1167112

Lee, C.-P., Hirata, N., Huang, B.-S., Huang, W.-G., & Tsai, Y.-B. (2010). Evidence of a highly attenuative aseismic zone in the active collision orogen of Taiwan. *Tectonophysics*, *489*(1–4), 128–138. https://doi.org/10.1016/j.tecto.2010.04.009

Lee, S.-J., Mozziconacci, L., Liang, W.-T., Hsu, Y.-J., Huang, W.-G., & Huang, B.-S. (2013). Source complexity of the 4 March 2010 Jiashian, Taiwan, earthquake determined by joint inversion of teleseismic and near field data. *Journal of Asian Earth Sciences*, *64*, 14–26. https://doi.org/10.1016/j.jseaes.2012.11.018

Lin, C.-H. (2002). Active continental subduction and crustal exhumation: The Taiwan orogeny. *Terra Nova*, *14*(4), 281–287. https://doi.org/10.1046/j.1365-3121.2002.00421.x

Marsan, D., & Wyss, M. (2011). Seismicity rate changes. *Community Online Resource for Statistical Seismicity Analysis*. https://doi.org/10.5078/corssa-25837590, http://www.corssa.org

Matthews, M. V., & Reasenberg, P. A. (1988). Statistical methods for investigating quiescence and other temporal seismicity patterns. *Pure and Applied Geophysics*, *126*(2–4), 357–372. https://doi.org/10.1007/BF00879003

Nadeau, R. M., & Dolenc, D. (2005). Nonvolcanic tremors deep beneath the San Andreas Fault. *Science*, *307*(5708), 389–389. https://doi.org/10.1126/science.1107142

Nadeau, R. M., & Guilhem, A. (2009). Nonvolcanic tremor evolution and the San Simeon and Parkfield, California, earthquakes. *Science*, *325*(5937), 191–193. https://doi.org/10.1126/science.1174155

Obara, K. (2002). Nonvolcanic deep tremor associated with subduction in Southwest Japan. *Science*, *296*(5573), 1679–1681. https://doi.org/10.1126/science.1070378

Obara, K., & Kato, A. (2016). Connecting slow earthquakes to huge earthquakes. *Science*, *353*(6296), 253–257. https://doi.org/10.1126/science.aaf1512

Ogata, Y. (2011). Significant improvements of the space-time ETAS model for forecasting of accurate baseline seismicity. *Earth, Planets and Space*, *63*(3), 6. https://doi.org/10.5047/eps.2010.09.001

Ohmi, S., & Obara, K. (2002). Deep low-frequency earthquakes beneath the focal region of the M_w 6.7 2000 Western Tottori earthquake. *Geophysical Research Letters*, *29*(16), 1807. https://doi.org/10.1029/2001GL014469

Parsons, T. (2004). Recalculated probability of $M \geq 7$ earthquakes beneath the sea of Marmara, Turkey. *Journal of Geophysical Research*, *109*, B05304. https://doi.org/10.1029/2003JB002667

Payero, J. S., Kostoglodov, V., Shapiro, N., Mikumo, T., Iglesias, A., Pérez-Campos, X., & Clayton, R. W. (2008). Nonvolcanic tremor observed in the Mexican subduction zone. *Geophysical Research Letters*, *35*, L07305. https://doi.org/10.1029/2007GL032877

Peng, W., & Toda, S. (2015). A new algorithm to find earthquake clusters using neighboring cell connection and rate analysis. In AGU Fall Meeting Abstracts.

Peng, Z., & Chao, K. (2008). Non-volcanic tremor beneath the central range in Taiwan triggered by the 2001 M_w 7.8 Kunlun earthquake. *Geophysical Journal International*, *175*(2), 825–829. https://doi.org/10.1111/j.1365-246X.2008.03886.x

Peterson, C. L., & Christensen, D. H. (2009). Possible relationship between nonvolcanic tremor and the 1998–2001 slow slip event, south Central Alaska. *Journal of Geophysical Research*, *114*, B06302. https://doi.org/10.1029/2008JB006096

Rogers, G., & Dragert, H. (2003). Episodic tremor and slip on the Cascadia subduction zone: The chatter of silent slip. *Science*, *300*(5627), 1942–1943. https://doi.org/10.1126/science.1084783

Rubinstein, J. L., Gomberg, J., Vidale, J. E., Wech, A. G., Kao, H., Creager, K. C., & Rogers, G. (2009). Seismic wave triggering of nonvolcanic tremor, episodic tremor and slip, and earthquakes on Vancouver Island. *Journal of Geophysical Research*, *114*, B00A01. https://doi.org/10.1029/2008JB005875

Schwartz, S. Y. (2015). Episodic aseismic slip at plate boundaries. In *Treatise on Geophysics* (2nd ed., pp. 445–465). Oxford: Elsevier. https://doi.org/10.1016/B978-0-444-53802-4.00084-1

Shelly, D. R. (2009). Possible deep fault slip preceding the 2004 Parkfield earthquake, inferred from detailed observations of tectonic tremor. *Geophysical Research Letters*, *36*, L17318. https://doi.org/10.1029/2009GL039589

Shelly, D. R. (2010). Migrating tremors illuminate complex deformation beneath the seismogenic San Andreas fault. *Nature*, *463*(7281), 648–652. https://doi.org/10.1038/nature08755

Shelly, D. R., Beroza, G. C., & Ide, S. (2007). Non-volcanic tremor and low-frequency earthquake swarms. *Nature*, *446*(7133), 305–307. https://doi.org/10.1038/nature05666

Shelly, D. R., Beroza, G. C., Ide, S., & Nakamula, S. (2006). Low-frequency earthquakes in Shikoku, Japan, and their relationship to episodic tremor and slip. *Nature*, *442*(7099), 188–191. https://doi.org/10.1038/nature04931

Shelly, D. R., Peng, Z., Hill, D. P., & Aiken, C. (2011). Triggered creep as a possible mechanism for delayed dynamic triggering of tremor and earthquakes. *Nature Geoscience*, *4*(6), 384–388. https://doi.org/10.1038/ngeo1141

Shih, M.-H., Huang, B.-S., Zhu, L., Yen, H.-Y., Tao-Ming, C., Win-Gee, H., & Chien-Ying, W. (2014). Fault orientation determination for the 4 March 2008 Taoyuan earthquake from dense near-source seismic observations. *TAO: Terrestrial, Atmospheric and Oceanic Sciences*, *25*(5), 637. https://doi.org/10.3319/TAO.2014.05.19.01(T

Sibson, R. H. (2009). Rupturing in overpressured crust during compressional inversion—The case from NE Honshu, Japan. *Tectonophysics*, *473*(3–4), 404–416. https://doi.org/10.1016/j.tecto.2009.03.016

Sibson, R. H., & Rowland, J. V. (2003). Stress, fluid pressure and structural permeability in seismogenic crust, North Island, New Zealand. *Geophysical Journal International*, *154*(2), 584–594. https://doi.org/10.1046/j.1365-246X.2003.01965.x

Teng, L. S., Lee, C. T., Tsai, Y. B., & Hsiao, L.-Y. (2000). Slab breakoff as a mechanism for flipping of subduction polarity in Taiwan. *Geology*, *28*(2), 155–158. https://doi.org/10.1130/0091-7613(2000)28<155:SBAAMF>2.0.CO;2

Toyokuni, G., Zhao, D., & Chen, K. H. (2016). Tomography of the source zone of the 2016 South Taiwan earthquake. *Geophysical Journal International*, *207*(1), 635–643. https://doi.org/10.1093/gji/ggw304

Wang, Y.-J., Ma, K.-F., Mouthereau, F., & Eberhart-Phillips, D. (2010). Three-dimensional Q_p-and Q_s-tomography beneath Taiwan orogenic belt: Implications for tectonic and thermal structure. *Geophysical Journal International*, *180*(2), 891–910. https://doi.org/10.1111/j.1365-246X.2009.04459.x

Wech, A. G., Boese, C. M., Stern, T. A., & Townend, J. (2012). Tectonic tremor and deep slow slip on the alpine fault. *Geophysical Research Letters*, *39*, L10303. https://doi.org/10.1029/2012GL051751

Wells, D. L., & Coppersmith, K. J. (1994). New empirical relationships among magnitude, rupture length, rupture width, rupture area, and surface displacement. *Bulletin of the Seismological Society of America*, *84*(4), 974–1002.

Wessel, P., & Smith, W. H. (1995). New version of the generic mapping tools. *Eos, Transactions American Geophysical Union*, *76*(33), 329–329. https://doi.org/10.1029/95EO00198

Wu, Y.-M., Chang, C.-H., Zhao, L., Teng, T.-L., & Nakamura, M. (2008). A comprehensive relocation of earthquakes in Taiwan from 1991 to 2005. *Bulletin of the Seismological Society of America*, *98*(3), 1471–1481. https://doi.org/10.1785/0120070166